navigation rms errors. A better albeit higher mean-squared error prediction results from the use of a stochastic description for the vehicle acceleration.

References

[1] Cannon, R. H., Jr., "Alignment of inertial guidance systems by gyrocompassing—linear theory," J. Aerospace Sci. **28**, 885–895, 912 (1961).

[2] McMurray, L. R., "Alignment of an inertial autonavigator," ARS J. **31**, 356–360 (1961).

[3] Narendra, K. S., "Pole-zero configurations and transient response of linear systems," TR 299, Cruft Lab., Harvard Univ. (May 1959).

[4] Draper, C. S., McKay, W., and Lees, S., *Instrument Engineering* (McGraw-Hill Book Co. Inc., New York, 1953), Vol. 2, p. 265.

[5] Newton, G. C., Jr., Gould, L. A., and Kaiser, J. F., *Analytical Design of Linear Feedback Controls* (John Wiley and Sons, Inc., New York, 1957), Appendix E, pp. 366–381.

[6] Roitenberg, I. N., "The accelerated placing of a gyroscopic compass in a meridian," J. Appl. Math. Mech. **23**, no. 5, 1370–1374 (1959).

[7] Friedman, A. L., "The use of speed and position fix information in inertial navigators," ARS Preprint 1957-61 (August 1961).

[8] Gelb, A. and Sandberg, H. J., "Finding system settling time," Control Eng. **9**, 103–104 (November 1962).

[9] Pitman, G. R., Jr., *Inertial Guidance* (John Wiley and Sons, Inc., New York, 1962), Chap. 8, pp. 176–209.

SEPTEMBER 1963 AIAA JOURNAL VOL. 1, NO. 9

Optimum Transfers between Hyperbolic Asymptotes

FRANK W. GOBETZ*

United Aircraft Corporation, East Hartford, Conn.

An investigation was made to determine the possible benefits of a single high-thrust impulse during the hyperbolic encounter of a spacecraft with a perturbing planet. The equations are formulated to allow for the application of the method to any two- or three-dimensional hyperbolic transfer problem; thus, applications require knowledge only of the hyperbolic excess velocities and the total turning angle of the maneuver. For cases in which the planetary radius enforces a constraint on the closest approach distance, generalized charts are presented to indicate the attendant performance penalty that is imposed. In addition to the single-impulse transfers, a four-impulse maneuver is described. This maneuver has the advantage of reducing performance requirements as well as increasing the time spent in the vicinity of the planet.

Nomenclature

A,B,C	=	coefficients of quadratic equation [Eq. (A6)]
a	=	semimajor axis
F	=	prime focus; center of gravitational attraction
R	=	planet radius
r	=	length of radius vector
V	=	velocity
ΔV	=	characteristic velocity requirement of maneuver
α	=	angular change of velocity vector at impulse point
β	=	angle between incoming asymptotes
η	=	true anomaly
θ	=	path angle
κ	=	total turning angle of transfer maneuver
μ	=	gravitational parameter
ψ	=	complement of half angle of hyperbola (see Fig. 3)

Subscripts

a	=	approach
d	=	departure
p	=	closest approach
v	=	Venus
1	=	incoming hyperbola
2	=	outgoing hyperbola
∞	=	infinity relative to planet (sphere of influence)

Introduction

SEVERAL schemes have been advanced which use the perturbing effect of a celestial body to induce a velocity increment in a space vehicle. Lawden[1] has shown that about 50% of the heliocentric velocity changes required to effect Hohmann transfers to Venus and Mars can be obtained by perturbation maneuvers involving the Earth's moon. Crocco[2] has planned a 14-month round-trip interplanetary voyage to Venus and Mars during which propulsion is required only at Earth departure and Earth arrival. In this case, trajectory variations induced by close approaches to the planets allow the probe to rendezvous with Earth on the homebound leg of the trip. These two examples differ in one fundamental respect, namely, that in the first case the perturbation is sought deliberately, whereas in the second case it is inevitable. Nevertheless, in both cases the perturbation is used to good advantage.

In order to capitalize further on maneuvers of this type, it would be useful to investigate the possible benefits of applying thrust impulses during the hyperbolic encounter with a perturbing body. This problem has been considered previously in Ref. 3. In that study the optimum point for minimizing characteristic velocity was defined for single-impulse transfers, but no general numerical results were presented. Also, no allowance was made for a constraint on the closest approach distance during the encounter. Since such a constraint is a significant consideration, optimum solutions of the constrained problem are desirable. The purpose of this study was to extend the optimum solutions of Ref. 3 to constrained conditions and to examine the desirability of using a multi-impulse maneuver to effect the transfer.

Discussion of Problem

The general three-body problem can be well approximated (for space flight purposes) as a succession of two-body prob-

Presented at the AIAA Astrodynamics Conference, New Haven, Conn., August 19–21, 1963.

* Research Laboratories. Associate Member AIAA.

lems wherein the focus of the vehicle's conic trajectory at any point is determined by the sphere of influence which encloses the vehicle at that time. For convenience in the discussion that follows, the sun is referred to as the major attracting body, and the perturbing body is Venus.

Consider first a heliocentric trajectory that intersects the Venusian orbit simultaneously with the arrival of the planet. As the vehicle enters Venus' sphere of influence, the frame of reference changes from a heliocentric to a planetocentric one. If the vehicle's heliocentric velocity at this point is $\bar{V}_a$ and the planet's velocity is $\bar{V}_v$, then the velocity of the vehicle relative to Venus is $\bar{V}_\infty = \bar{V}_a - \bar{V}_v$ (Fig. 1). The vehicle now approaches Venus along a hyperbola, one asymptote of which is an extension of the vector $\bar{V}_{\infty 1}$. The distance of closest approach to the planet can be regulated by properly timing the transit of the sphere of influence or by applying very small navigational corrections while the approaching spacecraft is still effectively at infinity relative to Venus. The net effect of such a correction is to translate $\bar{V}_{\infty 1}$ parallel to itself.

As shown in Fig. 1, the perturbation rotates the velocity vector by an angle 2ψ while leaving its magnitude unchanged, i.e., $V_{\infty 1} = V_{\infty 2}$. The degree of rotation is determined by the approach distance as well as by the magnitude of $\bar{V}_{\infty 1}$, whereas the desired sense of rotation can be obtained by approaching the planet from the correct side. The completed vector diagram illustrates the resultant deviation of the heliocentric trajectory from $\bar{V}_a$ to $\bar{V}_d$ when the frame of reference reverts back to the sun. In this diagram the relative magnitudes of the vectors have been exaggerated purposely in order to illustrate that the new velocity $\bar{V}_d$ is different from $\bar{V}_a$ in both magnitude and direction.

As previously stated, the rotation of $\bar{V}_{\infty 1}$ depends upon its magnitude and the distance of closest approach to Venus. For a fixed $\bar{V}_{\infty 1}$, the approach distance can vary but only within limits, since the planet has finite dimensions. Thus the deviation of $\bar{V}_a$ ranges from zero, when the sphere of influence is not penetrated and the planetocentric hyperbola degenerates to a straight line, to some maximum deviation, when the vehicle skims the planet's surface.

Consider now the case where vectors $\bar{V}_a$ and $\bar{V}_d$ are fixed, perhaps by the necessity of originating from and returning to Earth. Because of the limited effect of the perturbation maneuver, the transition from $\bar{V}_a$ to $\bar{V}_d$ will not be possible, in general, without the use of propulsion in addition to the perturbation. Since the velocity of the vehicle increases during the planetary approach, this propulsion is applied most effectively during the hyperbolic encounter and not when the motion is heliocentric.

With $\bar{V}_v$, $\bar{V}_a$, and $\bar{V}_d$ known, the problem becomes one of transferring from an approach hyperbolic velocity vector $\bar{V}_{\infty 1}$ to a departure velocity $\bar{V}_{\infty 2}$, where $\bar{V}_{\infty 1}$ and $\bar{V}_{\infty 2}$ are generally unequal in magnitude. The transfer takes place entirely within the planet's sphere of influence and is actually a transfer between the asymptotes of two planet-centered hyperbolas. By first considering the problem in two dimensions and leaving the magnitude, direction, and point of application of the impulse unspecified, it is possible to effect a transfer between any two hyperbolas and therefore between any two heliocentric trajectories. Subsequently, it will be shown that the three-dimensional problem always can be reduced to two dimensions so that the solution described here is quite general.

Admissible Solutions

In order to keep the characteristic velocity requirement of the thrust impulse ΔV from becoming too great, only one class of single-impulse solutions will be allowed. The total turning angle from $\bar{V}_{\infty 1}$ to $\bar{V}_{\infty 2}$ should never exceed 180°, for if it does the transfer can be performed more easily by passing to the opposite side of the planet, as illustrated in

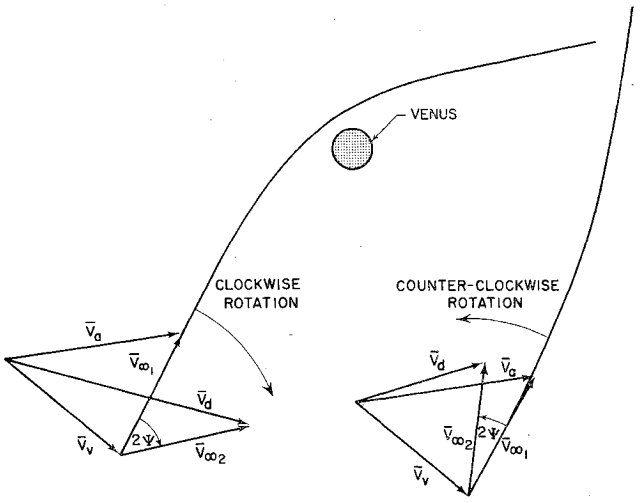

Fig. 1 Effect of hyperbolic encounter on heliocentric velocity vectors.

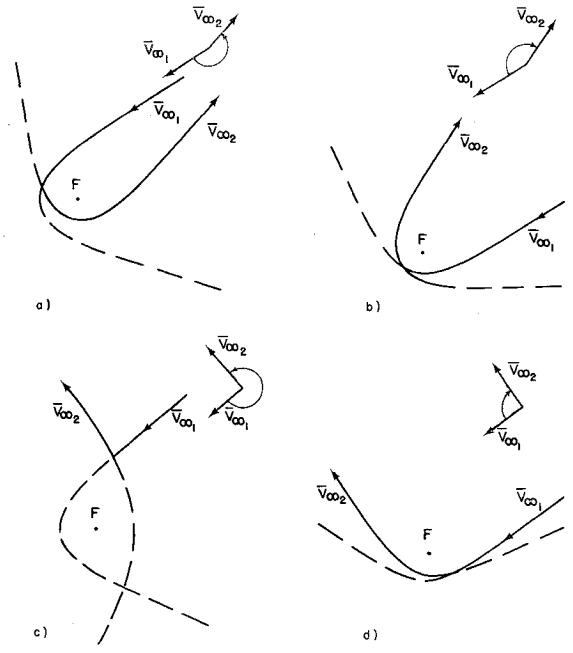

Fig. 2 Admissible transfers.

Fig. 2. In this figure the actual path of the probe is denoted by a solid curve, and the extension of each hyperbola is indicated by dashes. The first method (Fig. 2a) of transferring between $\bar{V}_{\infty 1}$ and $\bar{V}_{\infty 2}$ requires a counterclockwise rotation of greater than 180°. In the second case (Fig. 2b), the incoming asymptote has been translated parallel to itself by means of a prior correction so as to result in a clockwise rotation of the trajectory which is clearly superior to the first case. A similar argument applies in Figs. 2c and 2d. Thus, the hyperbolas always can be chosen such that the transfer angle does not exceed 180°, and when they are so chosen there exists but one intersection point at which to effect the transfer. In the limiting case of a 180° rotation, the incoming and outgoing asymptotes are parallel; however, there still exists but one intersection.

Analysis

The geometry of a single-impulse transfer between hyperbolic asymptotes is illustrated in Fig. 3. The hyperbolic excess velocity $\bar{V}_{\infty 1}$ of the approach hyperbola S-A-S' is directed along the incoming asymptote S-A. At point T the coplanar transfer is effected to hyperbola P-L-P', resulting in a total turning angle κ between $\bar{V}_{\infty 1}$ and $\bar{V}_{\infty 2}$.

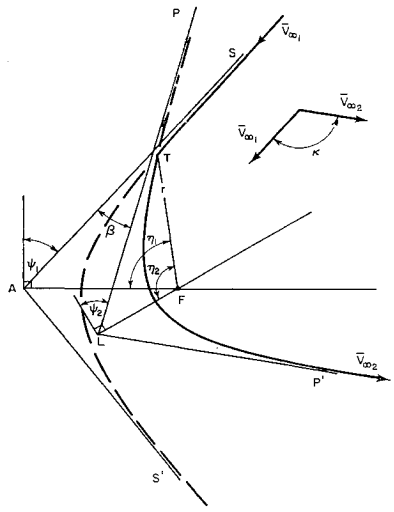

Fig. 3 Geometry of hyperbolic transfer maneuver.

In this illustration the probe transfers from the incoming leg of the first hyperbola to the incoming leg of the second hyperbola. The transfer also might take place between incoming and outgoing, between outgoing and incoming, or between outgoing and outgoing legs. The four possible modes of transfer are depicted in Fig. 4.

During this maneuver the total turning angle κ is the sum of the angle β between the two incoming asymptotes and the turning angle $2\psi_2$ of the second hyperbola:

$$\kappa = \beta + 2\psi_2 \tag{1}$$

From the geometry of the diagrams in Fig. 4, it can be shown that

$$\beta = \psi_1 - \psi_2 + \eta_2 - \eta_1 \tag{2}$$

in each case. (The true anomalies η_1 and η_2 are defined positive for clockwise rotations from the axes of symmetry and negative for counterclockwise rotations.) Now combining Eqs. (1) and (2) yields

$$\kappa = \psi_1 + \psi_2 + \eta_2 - \eta_1 \tag{3}$$

regardless of the mode of transfer.

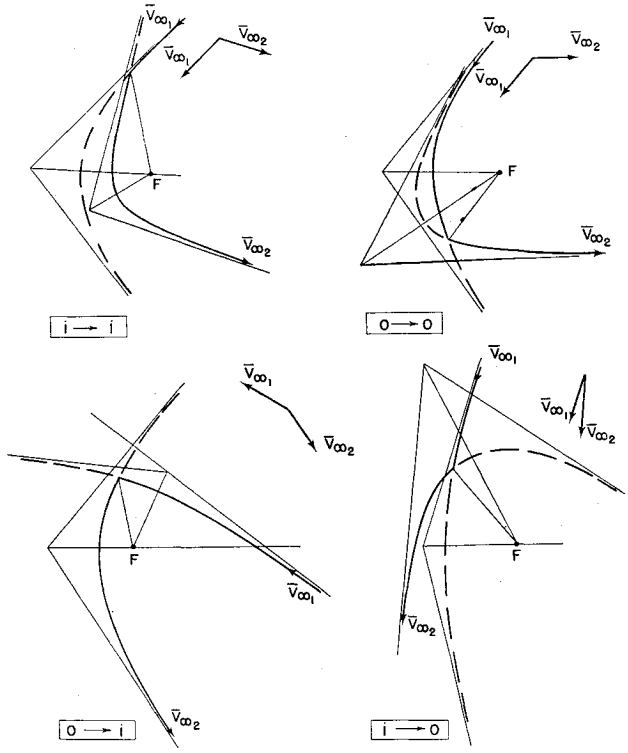

Fig. 4 Modes of transfer between hyperbolic asymptotes.

When Eq. (3), which is derived from the geometry of the problem, is used in combination with the standard equations for the path angle, velocity, and true anomaly of a conic (see Appendix A), the result is an expression for the performance factor $\Delta V/V_{\infty 1}$ as a function of the two independent variables ψ_1 and ψ_2. Using this equation, a computer program was written so that general solutions could be obtained for any transfer.

Special Solutions

Before proceeding to a discussion of the general solutions, two special sets of solutions will be considered. One of these will be referred to as the set of optimum transfers and is defined as the locus of transfers for which $\Delta V/V_{\infty 1}$ is minimized by optimal selection of the independent variables. No regard is given to the distance of closest approach to the center of force in these transfers, so that many of them are not generally feasible. The second special set contains only apsidal transfers, a case that involves two further constraints on the transfer maneuver. Since the impulse must be applied at the periapsides of both hyperbolas and tangent to the flight path, $\Delta V/V_{\infty 1}$ is uniquely determined for any transfer of this type. Development of the equations for this set of solutions, which will be referred to as periapsis transfers, is presented in Appendix B.

Summaries of these two special sets of solutions are presented in Figs. 5 and 6. In these figures the input parameters, consisting of the turning angle κ and velocity ratio $V_{\infty 2}/V_{\infty 1}$, appear as coordinates, and the important output information appears as curves of constant performance $\Delta V/V_{\infty 1}$ and nondimensional approach distance parameter $r_p V_{\infty 1}^2/\mu$. It is apparent that, for velocity ratios $V_{\infty 2}/V_{\infty 1}$ which are reciprocals of one another, "image" solutions occur, requiring equal values of ΔV. Therefore, only velocity ratios greater than or equal to unity are included in Figs. 5 and 6.

The two families of periapsis transfer curves in Fig. 5 are bounded by straight lines on the left and also on top and bottom. The straight line at the left ($V_{\infty 2}/V_{\infty 1} = 1$) designates the limiting case when the hyperbolic excess speeds are equal and the transfer can be performed without an impulse by selecting the proper approach angle:

$$\psi_1 = \psi_2 = \kappa/2 \tag{4}$$

The lower bound in Fig. 5 represents the degenerate case of an unperturbed or straight-line trajectory. Here the impulse is applied beyond the sphere of influence, and the velocity vector is changed in magnitude by the impulse but not in direction.

The upper bound is designated by $\kappa = 180°$, $r_p V_{\infty 1}^2/\mu = 0$, and $\Delta V/V_{\infty 1} = 0$. This corresponds to a trajectory that passes through the focus and for which no impulse is necessary. In practice, of course, the upper bound is determined by the radius of the perturbing planet.

The summary plot of optimum transfers in Fig. 6 is similar to Fig. 5, but certain basic differences exist. By definition, optimum transfers require smaller performance factors than periapsis transfers. Consequently, the curves of constant $\Delta V/V_{\infty 1}$ in Fig. 6 are shifted to the upper left relative to Fig. 5. Dissimilarities also are evident for the limiting angle $\kappa = 0$, i.e., the lower boundaries of the two diagrams. For $\kappa = 0$, periapsis transfers take place exclusively at infinity, whereas the approach parameter for optimum transfers varies with the velocity ratio. Thus the curves for constant $r_p V_{\infty 1}^2/\mu$ in Fig. 5 have gentle slopes and do not intercept the $V_{\infty 2}/V_{\infty 1}$ axis. In Fig. 6, these curves originate at the same points on the left-hand boundary $V_{\infty 2}/V_{\infty 1} = 1$ but slope steeply down to the right and intercept the $V_{\infty 2}/V_{\infty 1}$ axis.

General Solutions

As has been explained previously, the optimum single-impulse transfer is a valid solution only when the closest

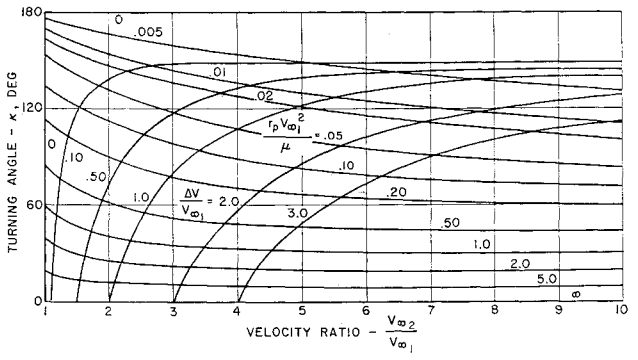

Fig. 5 Summary plot of periapsis transfers.

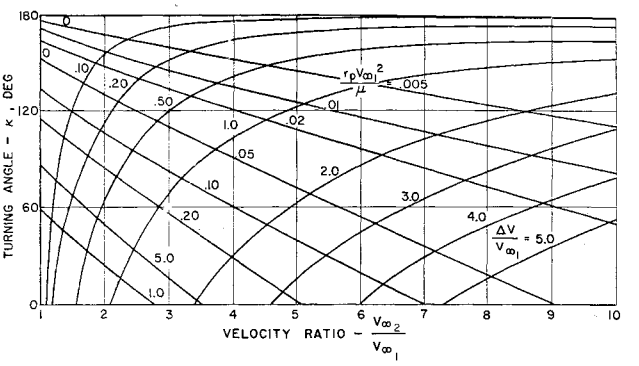

Fig. 6 Summary plot of optimum transfers.

approach distance is greater than the radius of the perturbing planet or of the extremities of its atmosphere. When this condition is violated, a constrained optimum solution must be sought. It is also conceivable that, for a particular mission, the approach distance itself could be an input item. Therefore, the results of the numerical calculations have been presented in Figs. 7–13 with $\Delta V/V_{\infty 1}$ as ordinate and $r_p V_{\infty 1}^2/\mu$ as abscissa. In each figure the turning angle κ has been fixed, and the solid curves are loci of constant $V_{\infty 2}/V_{\infty 1}$.

In discussing the significance of these solutions, Figs. 7 and 13 corresponding to $\kappa = 0°$ and $\kappa = 180°$ will be disregarded temporarily so that they can be viewed subsequently as special cases.

As a starting point, consider Fig. 10, for which $\kappa = 90°$. Note that each solid curve, representing a constant ratio $V_{\infty 2}/V_{\infty 1}$, has a horizontal asymptote as $r_p V_{\infty 1}^2/\mu$ becomes infinite. These asymptotes are defined by the equation

$$\frac{\Delta V}{V_{\infty 1}} = \left[\left(\frac{V_{\infty 2}}{V_{\infty 1}}\right)^2 + 1 - 2\,\frac{V_{\infty 2}}{V_{\infty 1}}\cos\kappa\right]^{1/2} \qquad (5)$$

Thus, the transfers approach a condition where the impulse is applied at infinity (beyond the sphere of influence), and no encounter occurs. As closer approaches are made, $\Delta V/V_{\infty 1}$ decreases to a minimum and then increases. But before the minimum is reached the curves pass through the locus of periapsis transfers which is designated by a dashed line. If still closer approaches are desired, $\Delta V/V_{\infty 1}$ must be increased again, until for $r_p V_{\infty 1}^2/\mu = 0$ the curves would approach a horizontal asymptote. This asymptote corresponds to a unit eccentric hyperbola passing through the focus followed (or preceded) by an impulse at infinity to accomplish the desired rotation of the hyperbolic velocity vector. The performance factor at $r_p V_{\infty 1}^2/\mu = 0$ is expressed by Eq. (6):

$$\frac{\Delta V}{V_{\infty 1}} = \left[\left(\frac{V_{\infty 2}}{V_{\infty 1}}\right)^2 + 1 + 2\,\frac{V_{\infty 2}}{V_{\infty 1}}\cos\kappa\right]^{1/2} \qquad (6)$$

An interesting feature of these solutions is the fact that the region to the right of the periapsis line in Fig. 10 contains only transfers of the type 0-0, illustrated in Fig. 4. Thus, the vehicle approaches the planet on the incoming hyperbola and does not transfer to the second hyperbola until after it has passed through periapsis of the first. To the left of the periapsis line is a region composed of *i-i* transfers. This region includes the locus of optimum transfers, illustrating that all optimum transfers are of the *i-i* type when the ratio $V_{\infty 2}/V_{\infty 1} > 1$. Conversely, when $V_{\infty 2}/V_{\infty 1} < 1$, the regions are reversed. At least one other change in the type of transfer may occur beyond the locus of optimum transfers, but this region is of limited interest.

The curve for $V_{\infty 2}/V_{\infty 1} = 1$ is of special interest because it contains as a limiting case the hyperbolic encounter without propulsion, i.e., $\Delta V/V_{\infty 1} = 0$. Significantly, the loci of optimum and periapsis transfers also approach this point as $V_{\infty 2}/V_{\infty 1} \to 1$. When this ratio is unity there is no advantage to be gained by applying the impulse during the encounter, since no change in hyperbolic velocity is desired. The encounter still occurs, however, satisfying at least part of the change in direction between $V_{\infty 1}$ and $V_{\infty 2}$. Since the impulse can be applied either before or after the encounter, this solution does not violate the forementioned rule designating the regions of *i-i* and 0-0 transfers.

The other figures in this group indicate the effect of varying the turning angle. Considering first angles less than 90° (Figs. 7–9), note the steady increase of the approach distance parameter as κ goes to zero. Also note that the locus of periapsis transfers gradually moves to the right until, for $\kappa = 0$, such transfers correspond to $r_p V_{\infty 1}^2/\mu = \infty$. For turning angles greater than 90° (Figs. 11–13), the opposite trend is evident, i.e., approach distances decrease and the locus curves move to the left.

When $\kappa = 180°$, this trend reaches a limit as the $\Delta V/V_{\infty 1} = 0$ point reaches $r_p V_{\infty 1}^2/\mu = 0$, and the locus of optimum as well as periapsis transfers shrinks to this point. The curves for all velocity ratios originate at the origin and increase slowly with increasing approach distance, but only the portion of these curves which corresponds to realistic approach distances is shown in Fig. 13.

Three-Dimensional Considerations

If the heliocentric velocity vectors $\bar{V}_a$, $\bar{V}_d$, and $\bar{V}_v$ are not coplanar, the resultant vector diagram is that illustrated in Fig. 14. Even though the problem is three-dimensional in heliocentric space, it always can be reduced to two dimensions in the planetary frame of reference. This is illustrated in Fig. 14b. The vectors $\bar{V}_{\infty 1}$ and $\bar{V}_{\infty 2}$ represent the hyperbolic excess velocities required to effect transfer from $\bar{V}_a$ to $\bar{V}_d$ in Fig. 14a. Point F is the center of attraction and therefore must coincide with the foci of the hyperbolas. By a prior correction, vector $\bar{V}_{\infty 1}$ can be translated arbitrarily in space so long as its new line of action is parallel to the previous one. The same applies to $\bar{V}_{\infty 2}$, although this correction would occur after the encounter. Therefore, the plane formed by the two vectors can be translated until it includes point F, and the transfer is then coplanar. Although the maneuver could, of course, be made to include more than one plane, it necessarily would require a higher ΔV; such a transfer would be pointless.

Four-Impulse Transfers

An objectionable feature of the manned probe mission is that the length of time spent in the vicinity of the target planet is very small compared to the total mission trip time. The transfers thus far considered here do not appreciably alter this situation because they involve only a single impulse. But if application of multiple impulses is allowed, the duration of the planetary stay time can be increased appreciably.

Consider the four-impulse transfer of Ref. 4 which is depicted in Fig. 15. The vehicle approaches on hyperbola

(*AP*), which has its periapsis just slightly above the planet's surface. Here at *P* a reverse tangential impulse establishes the vehicle in a highly eccentric elliptic orbit *PQ* such that the velocity of the probe will diminish to an extremely small value when the probe has receded far from the planet but still remains within its sphere of influence. Since its velocity is now negligibly small, an infinitesimally small impulse at *Q* transfers the probe from *PQ* to *QR*, and an equally small impulse at *R* places the probe back on another long ellipse *RP*. The final impulse, which, like the first, is tangential and finite, occurs at *P* to transfer the probe to hyperbola *PS*. It is apparent that, by increasing the number of infinitesimal impulses, variations on this maneuver may be conceived of. Since these variations will require equivalent values of $\Delta V/V_{\infty 1}$, however, the four-impulse transfer can be thought of as the basic multi-impulse maneuver.

In addition to prolonging stay time, this series of maneuvers makes the transfer independent of κ. Note that in Fig. 15 κ can be increased or decreased arbitrarily by adjusting the length of arc *QR*. It follows that, for certain combinations of κ and $V_{\infty 2}/V_{\infty 1}$, the four-impulse transfer can require a lower $\Delta V/V_{\infty 1}$ than the single-impulse case.

In calculating performance requirements for four-impulse transfers, the two small impulses are neglected. The magnitudes of the larger impulses are defined as the differences

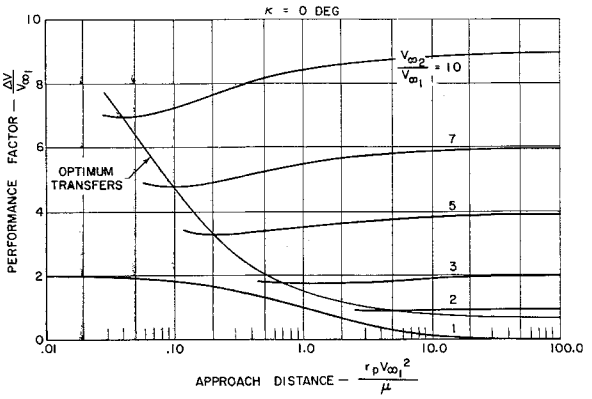

Fig. 7 Single-impulse transfers, 0°.

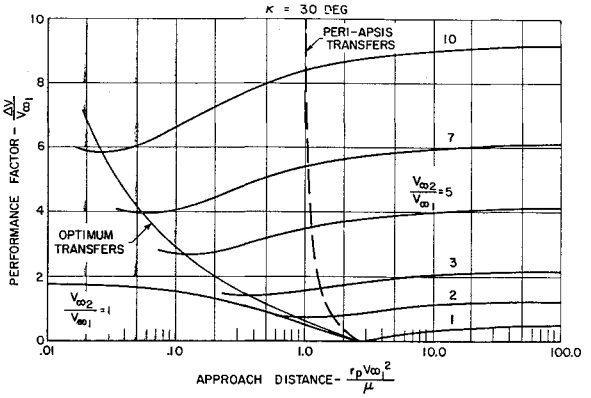

Fig. 8 Single-impulse transfers, 30°.

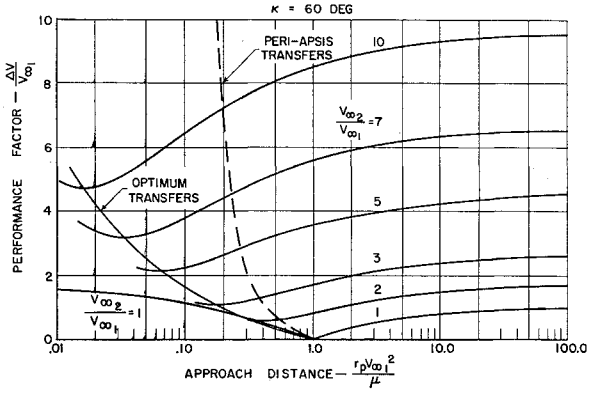

Fig. 9 Single-impulse transfers, 60°.

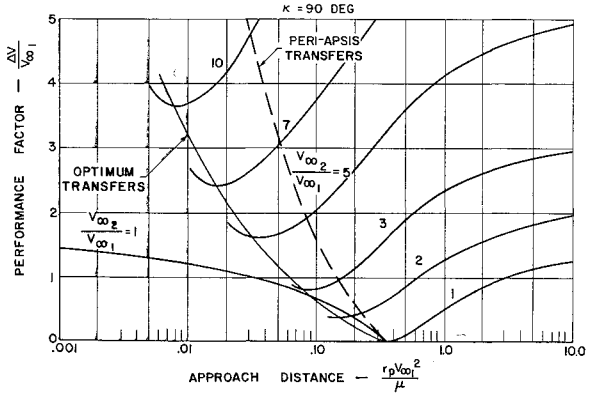

Fig. 10 Single-impulse transfers, 90°.

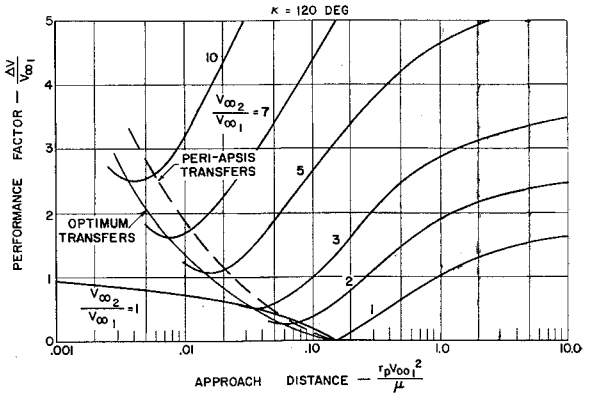

Fig. 11 Single-impulse transfers, 120°.

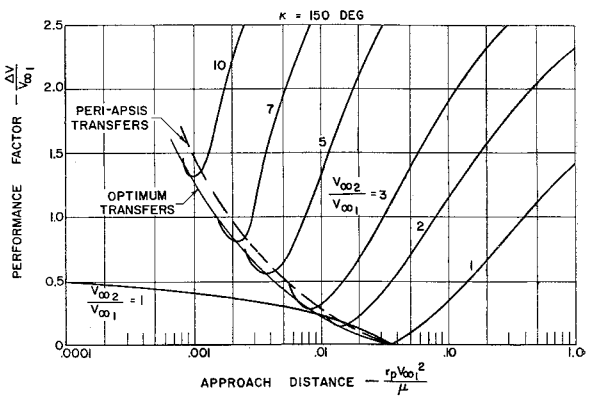

Fig. 12 Single-impulse transfers, 150°.

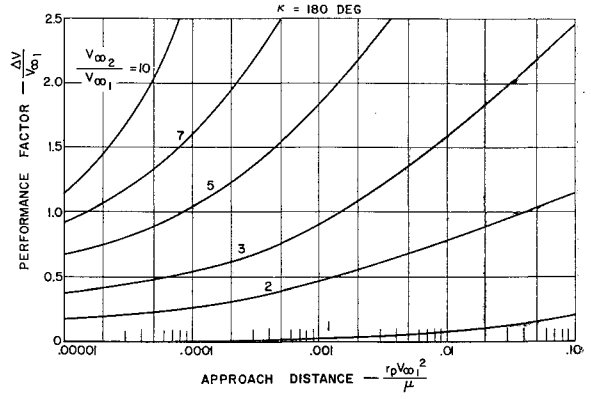

Fig. 13 Single-impule transfers, 180°.

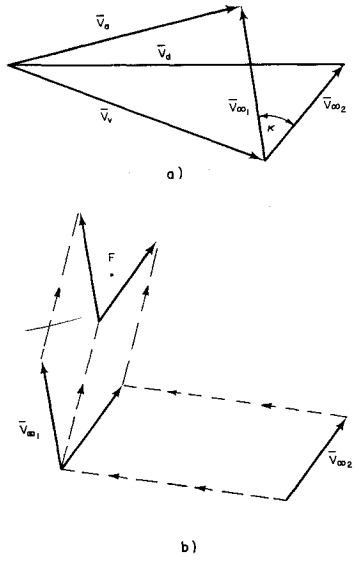

Fig. 14 Aspects of three - dimensional problem.

between escape velocity and periapsis velocities for the respective hyperbolas:

$$\frac{\Delta V}{V_{\infty 1}} = \left(1 + \frac{2}{r_p V_{\infty 1}^2/\mu}\right)^{1/2} + \left[\left(\frac{V_{\infty 2}}{V_{\infty 1}}\right)^2 + \frac{2}{r_p V_{\infty 1}^2/\mu}\right]^{1/2} - 2\left(\frac{2}{r_p V_{\infty 1}^2/\mu}\right)^{1/2} \quad (7)$$

A summary of four-impulse transfers based on Eq. (7) is given in Fig. 16, and an interesting comparison between these results and those for the optimum single-impulse transfers is presented in Fig. 17. In this plot, $r_p V_{\infty 1}^2/\mu$ is held fixed at an arbitrary value so that certain optimum single-impulse transfers are made impossible because a limit on approach distance is also a limit on the turning angle.

In Fig. 17 the region in which optimum or constrained optimum single-impulse transfers are superior (lower $\Delta V/V_{\infty 1}$) is the shaded region. The region of optimum single-impulse transfers is bounded at the top by the radius limitation. That is, the optimum single-impulse transfer would be superior for larger turning angles if the physical size of the planet did not prevent such transfers. On the lower boundary, $\Delta V/V_{\infty 1}$ for the optimum single- or four-impulse maneuvers is the same. The limit on approach distance does not exclude constrained optimum solutions, and in the region above the constraint line in Fig. 17 constrained optimum solutions are better than four-impulse transfers.

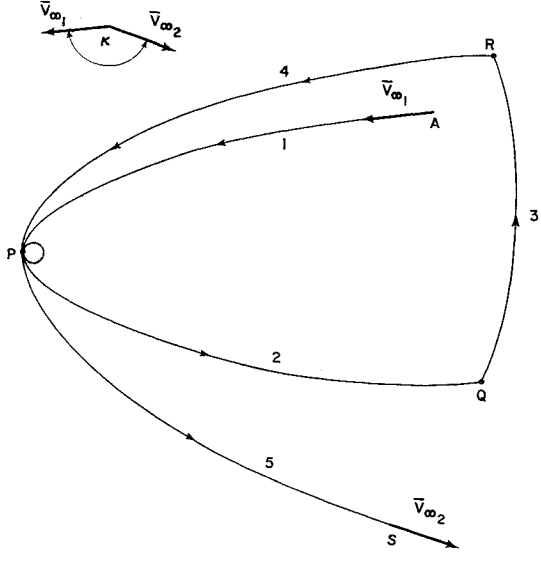

Fig. 15 Four-impulse transfer.

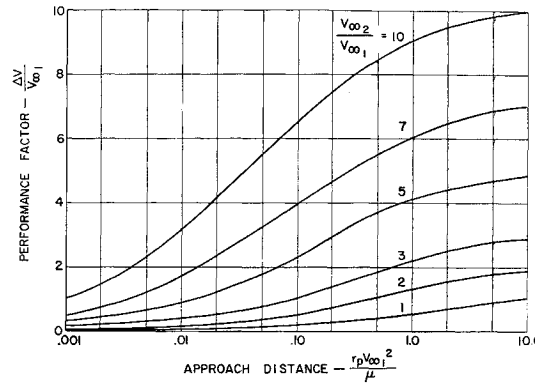

Fig. 16 Summary of four-impulse transfers.

As an aid in using the foregoing charts, Fig. 18 relates the minimum approach distance to incoming hyperbolic excess speed for several possible perturbing bodies. In Fig. 18, $RV_{\infty 1}^2/\mu$ represents the closest approach permissible for given $V_{\infty 1}$, based on the size of the perturbing body. For example, consider a hypothetical encounter with Venus where $V_{\infty 1} = 10{,}000$, $V_{\infty 2} = 50{,}000$, and $\kappa = 60°$. Figure 18 shows that for $V_{\infty 1} = 10{,}000$ the closest approach parameter is $RV_{\infty 1}^2/\mu = 0.155$, but from Fig. 9 for $V_{\infty 2}/V_{\infty 1} = 5$, $\kappa = 60°$ this constraint precludes an optimum transfer. Therefore, assuming the closest possible approach, $r_p V_{\infty 1}^2/\mu = 0.155$, $\Delta V/V_{\infty 1} = 2.46$, or $\Delta V = 24{,}600$.

Concluding Remarks

For purposes of mission analysis, the method presented here for analyzing single-impulse transfers should be quite adequate. Use of the two-body approximation to the three-body problem and the assumption of impulsive thrust application should be sufficiently close approximations for all but the most exact trajectory calculations.

Because the two-dimensional solution is also valid in a three-dimensional problem, the hyperbolic transfer maneuver can be included in computer programs for calculating interplanetary flyby trajectories. The equations that describe the maneuver itself (see Appendix A) involve no iterative procedures and could be integrated into a more general program without appreciable difficulty. A useful starting point in the numerical optimization of $\Delta V/V_{\infty 1}$ would be the periapsis transfer point because it is found easily and because it is never far from the optimum itself.

During the early phases of manned interplanetary flight, flyby probe missions will be performed involving close approaches to the nearby planets Venus and Mars. If useful experiments are to be performed in the vicinity of these planets, it is necessary that close approaches be made and that planetary perturbations be accounted for in planning the trajectories. Since these perturbations are inevitable

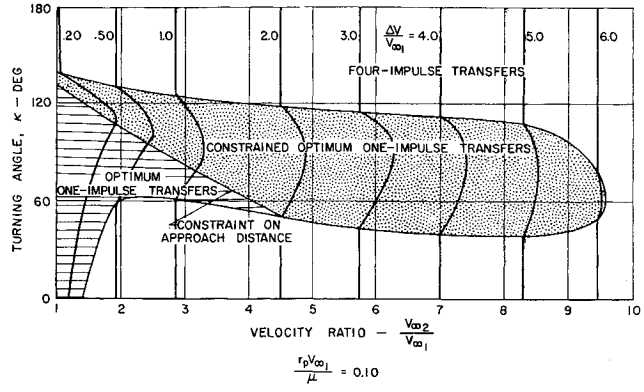

Fig. 17 Comparison of single-impulse with four-impulse transfers, $r_p V_{\infty 1}^2/\mu = 0.10$.

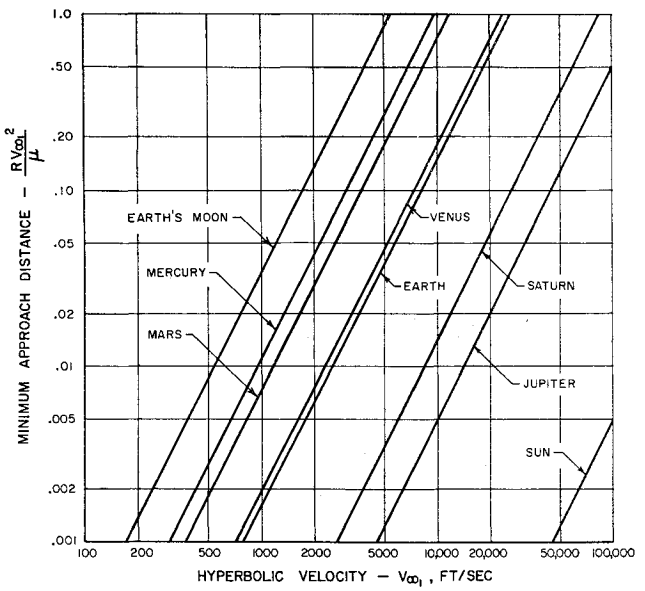

Fig. 18 Minimum approach distances for some perturbing bodies.

on such missions, it seems logical to take advantage of them to whatever degree possible. The planetary perturbation cannot, in itself, represent a large percentage of the total energy requirement of the mission, but the addition of a thrust impulse during the encounter could greatly increase mission flexibility. This benefit would be especially significant if a fast mission were desirable.

A considerable advantage also can be gained by performing a four-impulse maneuver in the vicinity of the target planet. This maneuver increases planetary stay time without greatly increasing the characteristic velocity requirement over the single-impulse transfer, and, for some cases, particularly for strong force fields, the four-impulse transfer actually reduces characteristic velocity.

Conclusions

1) Considerable reductions in characteristic velocity requirement are attainable by application of thrust impulses during the hyperbolic encounter rather than beyond the planet's sphere of influence. These reductions are especially great when the turning angle and the ratio between incoming and outgoing velocities are large.

2) Transfers that result in minimum fuel consumption are generally nontangential but are usually not practical because they would take place below the planetary surface.

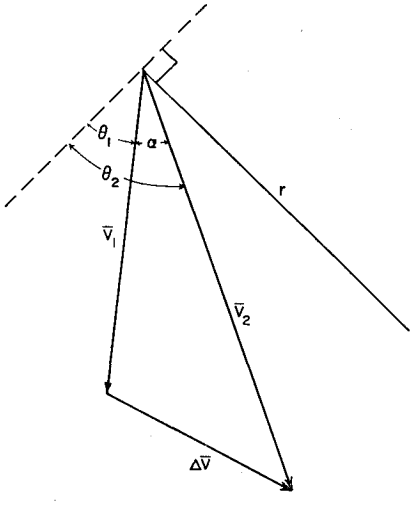

Fig. 19 Vector diagram of transfer maneuver.

3) In applications of the method described herein, the periapsis transfer is a useful starting point because it is found easily and because it is often close to the optimum solution.

4) The three-dimensional hyperbolic transfer problem can always be reduced to two dimensions without loss of generality.

5) The four-impulse transfer is often superior to the single-impulse case in terms of the characteristic velocity required for the maneuver, and it also allows increased time in the vicinity of the planet.

Appendix A: Derivation of Performance Equation

Focusing attention on the transfer maneuver itself, it is seen from Fig. 19 that, upon application of the impulse $\Delta\bar{V}$, the velocity vector $\bar{V}_1$ on the approach hyperbola is changed to $\bar{V}_2$ on the departure hyperbola. The angle α between $\bar{V}_1$ and $\bar{V}_2$ is the difference between the path angles θ_1 and θ_2, and the magnitude of $\Delta\bar{V}$ is determined easily:

$$\Delta V = (V_1^2 + V_2^2 - 2V_1V_2\cos\alpha)^{1/2} \tag{A1}$$

where

$$\alpha = \theta_2 - \theta_1 \tag{A2}$$

It was found that a great reduction in the complexity of the remaining equations could be obtained by choosing the angles ψ_1 and ψ_2 as the independent variables. If the major axis is represented by the parameter $a = \mu/V_\infty^2$, the angles θ and η can be written as

$$\theta = \pm\cos^{-1}\left(\frac{1}{\tan\psi\{(rV_\infty^2/\mu)[2 + (rV_\infty^2/\mu)]\}^{1/2}}\right) \tag{A3}$$

and

$$\eta = \pm\cos^{-1}\left[\sin\psi\left(\frac{1}{(rV_\infty^2/\mu)\tan^2\psi} - 1\right)\right] \tag{A4}$$

The path speed V is a function of r and a through the relation

$$V = \{\mu[(2/r) + (1/a)]\}^{1/2} \tag{A5}$$

Combining Eqs. (3 and A1–A5) and retaining only ψ_1 and ψ_2, the following equations are obtained:

$$\Delta V = \left(\frac{\mu}{a_1}\right)^{1/2}\left[1 + \frac{a_1}{a_2} + \frac{4}{r/a_1} - \frac{2(a_2/a_1)^{1/2}}{(r/a_1)^2\tan\psi_1\tan\psi_2}\times\left(1 + \left\{\left[\frac{r}{a_1}\left(2 + \frac{r}{a_1}\right)\tan^2\psi_1 - 1\right]\times\left[\frac{r}{a_2}\left(2 + \frac{r}{a_2}\right)\tan^2\psi_2 - 1\right]\right\}^{1/2}\right)\right]^{1/2} \tag{A6}$$

and

$$A(r/a_1)^2 + B(r/a_1) + C = 0 \tag{A7}$$

where the coefficients A, B, and C of the quadratic, Eq. (A7), are

$$A = [\cos(\kappa - \psi_1 - \psi_2) - \sin\psi_1\sin\psi_2]^2 - \cos^2\psi_1\cos^2\psi_2$$

$$B = 2\left[\cos(\kappa - \psi_1 - \psi_2)\frac{\cos\psi_1\cos\psi_2}{\tan\psi_1\tan\psi_2}\times\left(\frac{a_2}{a_1}\tan^2\psi_1 + \tan^2\psi_2\right) - \left(\frac{a_2}{a_1}\cos^2\psi_2 + \cos^2\psi_1\right)\right] \tag{A8}$$

$$C = \frac{\cos\psi_1\cos\psi_2}{\tan\psi_1\tan\psi_2}\left[\frac{\sin\psi_1}{\sin\psi_2}\left(\frac{a_2}{a_1}\frac{\cos\psi_2}{\cos\psi_1}\right)^2 + \frac{\sin\psi_2}{\sin\psi_1}\left(\frac{\cos\psi_1}{\cos\psi_2}\right)^2 - 2\frac{a_2}{a_1}\cos(\kappa - \psi_1 - \psi_2)\right]$$

By solving Eq. (A7) for r/a_1, the problem is reduced to one

equation in the two independent variables, ψ_1 and ψ_2. In addition, by forming the functions

$$\frac{\Delta V}{V_{\infty 1}} = \left(\frac{a_1 \Delta V^2}{\mu}\right)^{1/2} \qquad \frac{r V_{\infty 1}^2}{\mu} = \frac{r}{a_1} \tag{A9}$$

in Eq. (A6) the entire solution can be reduced to two input parameters: a_2/a_1 [or $(V_{\infty 1}/V_{\infty 2})^2$] and κ. The optimization is thus made independent of the planet and of the initial planetocentric velocity $V_{\infty 1}$.

Appendix B: Periapsis Transfer

If it is required that the impulse be applied tangentially at the periapsis, the equations of Appendix A are greatly simplified. When $\eta_1 = \eta_2 = 0$, it can be shown that

$$\frac{r}{a_1} = \frac{(a_2/a_1)(\sin\psi_2/\sin\psi_1)(\tan^2\psi_1/\tan^2\psi_2) - 1}{\tan^2\psi_1[(\sin\psi_2/\sin\psi_1) - 1]} \tag{B1}$$

$$\kappa = \psi_1 + \psi_2 \tag{B2}$$

$$\sin\psi_1\left(\frac{1}{(r/a_1)\tan^2\psi_1} - 1\right) = 1 \tag{B3}$$

Eliminating r/a_1 from Eqs. (B1) and (B2) produces an expression relating ψ_1 and ψ_2:

$$\sin\psi_1 = \frac{\sin\psi_2}{(a_2/a_1) + [1 - (a_2/a_1)]\sin\psi_2} \tag{B4}$$

Finally, the requirement that the impulse be tangential is expressed by

$$\cos\theta_1 = \cos\theta_2 \tag{B5}$$

and the equation for $\Delta V/V_{\infty 1}$ becomes

$$\frac{\Delta V}{V_{\infty 1}} = \left(1 + \frac{a_1}{a_2} + \frac{2}{r/a_1} \times \left[2 - \left\{\left(2 + \frac{r}{a_1}\right)\left(2 + \frac{a_1}{a_2}\frac{r}{a_1}\right)\right\}^{1/2}\right]\right)^{1/2} \tag{B6}$$

From Eqs. (B2) and (B4), the constraining equation is

$$\sin(\kappa - \psi_2) = \frac{\sin\psi_2}{(a_2/a_1) + [1 - (a_2/a_1)]\sin\psi_2} \tag{B7}$$

References

[1] Lawden, D. F., "Perturbation maneuvers," J. Brit. Interplanet. Soc. **13**, 329–334 (November 1954).

[2] Crocco, G. A., "One year exploration trip: Earth-Mars-Venus," *Proceedings of the VII International Astronautical Congress, Rome, September 17–22, 1956* (Proceedings of Roma, Associazione Italiana Razzi, Rome, 1956), pp. 227–252.

[3] Contensou, P., "Etude theorique des trajectoires optimales dans un champ de gravitation. Application au cas d'un centre d'attraction unique. (Theoretical study of optimal trajectories in a gravitational field. Application in the case of a single center of attraction)," Astronaut. Acta VIII, 2–3 (1963); also Grumman Res. Transl. TR-22 by P. Kenneth (August 1962).

[4] Edelbaum, T. N., "How many impulses," United Aircraft Corp. Res. Labs. Rept. A-110052-12 (in preparation).

[5] Ehricke, K. A., *Principles of Guided Missile Design—Space Flight* (D. Van Nostrand Co. Inc., Princeton, N. J., 1960), Chap. IV.

SEPTEMBER 1963 AIAA JOURNAL VOL. 1, NO. 9

Derivation of Nodal Period of an Earth Satellite and Comparisons of Several First-Order Secular Oblateness Results

FORD KALIL* AND FRED MARTIKAN†

The Martin Company, Baltimore, Md.

An expression for nodal period is derived to first order in the perturbed gravitational potential of an oblate earth spheroid, i.e., to order J and for small eccentricities $e = O(J_2)$. First-order secular effects on satellite motion around an oblate earth, as obtained by various authors, have been compared and found in agreement. However, some disagreement exists in the expressions obtained for the anomalistic and nodal period of satellite motion by various authors. A consistent set of expressions for these periods is recommended for use in orbital calculations.

Nomenclature

a = semimajor axis
a_0 = semimajor axis of a Keplerian orbit; unperturbed semimajor axis
$\bar{a}$ = mean semimajor axis of a perturbed orbit
b = constant defined by Eq. (8)
e = eccentricity, with a varying interpretation by different authors
e_0 = eccentricity constant
f = earth's flattening $\simeq 1/298.25$
h = satellite altitude
$\bar{h}$ = average satellite altitude in the region $0° \leq \beta < 360°$
i_0 = average orbit inclination about which i varies periodically; i_0 is measured positive in counterclockwise direction from due east on the equator to orbital plane at the ascending node, so that $0° \leq i_0 \leq 180°$
J_2 = second zonal harmonic coefficient in the expansion of earth's gravitational potential 1.08228×10^{-3}
k = constant defined by Eq. (3)
n_0 = mean motion of an unperturbed satellite orbit
n_r = perturbed anomalistic mean motion of a satellite

Received by ARS November 27, 1962; revision received June 3, 1963.

* Senior Engineering Specialist, Aerospace Mechanics Department; presently with NASA Goddard Spaceflight Center, Systems Analysis Office.

† Engineering Specialist, Aerospace Mechanics Department. Associate Member AIAA.